LAWRENCE
LIVERMORE
NATIONAL
LABORATORY

UCRL-JRNL-209584

Intrabasin Comparison of Surface Radiocarbon Levels in the Indian Ocean Between Coral Records and Three-Dimension Global Ocean Models

N. S. Grumet, P. B. Duffy, M. E. Wickett, K. Caldeira, R. B. Dunbar

February 10, 2005

Global Biogeochemical Cycles

Intrabasin Comparison of Surface Radiocarbon Levels in the Indian Ocean Between Coral Records and Three-Dimension Global Ocean Models

Nancy S. Grumet[1], Philip B. Duffy[2], Michael E. Wickett[3], Ken Caldeira[2], and Robert B. Dunbar[1]

[1]Department of Geological and Environmental Sciences, Stanford University, Stanford, California 94305
[2]Energy and Environment Directorate, Lawrence Livermore National Laboratory, Livermore, California 94551
[3]Center for Applied Scientific Computing, Lawrence Livermore National Laboratory, Livermore, California 94551

Abstract

Oceanic uptake and transport of bomb produced radiocarbon is used as a diagnostic in global ocean models to test parameterizations of mixing and air-sea gas exchange between the ocean and atmosphere. A model's ability to simulate bomb produced ^{14}C is also a good indicator of its ability to predict uptake of anthropogenic CO_2. We have conducted a model-data comparison of surface radiocarbon time-series from coral records from the coasts of Kenya and Sumatra and a suite of dynamical three-dimension ocean models that were included in the second phase of the Ocean Carbon-Cycle Model Intercomparison Project. The coral records comprise the first intrabasin record of surface water $\Delta^{14}C$ variability in the equatorial Indian Ocean and provide an independent evaluation of model performance. Differing treatments of lateral subgrid scale mixing in different models appear to be less important than other, unknown factors in explaining differences in results between the models. Those models that include a dynamic vertical mixing scheme appear to be more capable of matching observed coral radiocarbon time-series. Yet, among models with the same parameterization of lateral subgird scale mixing, there is a large degree of variation, suggesting that at both sites factors such as resolution, topography, physical forcing and horizontal advection are more important than mixing parameterization in explaining intermodel differences. None

of the models reproduce the time-lag in the rate of bomb ^{14}C response between the Kenya and Sumatra coral sites. Future efforts are needed to improve model simulation of radiocarbon in surface waters in the equatorial Indian Ocean.

1. Introduction

Models of the climate system, including land, atmosphere, and ocean components, are a principal tool in understanding and predicting climate change. The ocean's large capacity for the transport and storage of carbon plays a major role in controlling the concentration of atmospheric CO_2. Therefore, ocean models are used extensively to understand air-sea fluxes and ocean storage of anthropogenic carbon. The increasing demands put on Ocean General Circulation Models (OGCMs), involving prediction of changes in both the climate system and the carbon-cycle, require thorough evaluation of model performance.

An important tool for evaluating model performance is the simulation of the ocean's uptake of transient tracers, such as chlorofluorocarbons (CFCs) and radiocarbon (^{14}C), which enter the surface ocean via gas exchange and are transported throughout the ocean as passive tracers of circulation and mixing processes. The deep ocean is depleted in ^{14}C relative to the surface ocean due to the long residence time of deep ocean water, which allows for significant ^{14}C decay ($t_{1/2}$=5730 yrs). In contrast, the surface ocean is enriched in ^{14}C as a result of air-sea gas exchange processes. This enrichment makes the distribution of ^{14}C sensitive to vertical transport. This strong vertical gradient makes simulation of naturally-occurring ^{14}C a good test of ocean circulation models. Atmospheric nuclear weapons testing produced an excess of atmospheric ^{14}C that has augmented the difference between surface and deep ocean ^{14}C concentrations.

Simulation of the bomb ^{14}C perturbation is a valuable test of ocean circulation processes on decadal time-scales (e.g., Toggweiler et al., 1989; Duffy and Caldeira, 1995; Duffy et al., 1995a; Rodgers et al., 1997; Guilderson et al., 2000; Rodgers et al., 2000). It is also a diagnostic in OGCMs to test parameterizations of subgrid-scale mixing and air-sea gas exchange between the ocean and atmosphere (e.g., Duffy et al., 1995b; Jain et al., 1995; Duffy et al., 1997). Furthermore, a model's ability to simulate uptake of bomb ^{14}C is a good indicator of its ability to simulate uptake of anthropogenic CO_2, because the same physical processes (air-sea exchange and ocean circulation) are involved in both cases. The analogy between bomb ^{14}C and CO_2 is imperfect, however in part because radiocarbon isotopes have a longer air-sea equilibration time than molecular CO_2 (~10 years versus ~1 year) (Broecker and Peng, 1974).

Radiocarbon time-series from corals provide information about surface and shallow circulation that can be used to test ocean dynamics in circulation models. Differences between models and observed data reflect how well different models parameterize air-sea exchange and mixing. The timing and amplitude of the post-bomb peak is diagnostic of air-sea exchange processes and mixing of bomb $^{14}CO_2$ out of the surface mixed layer and into the deep reservoir (Guilderson et al., 2000) as well as other aspects of ocean circulation. In this research we examine how well models simulate these processes in the Indian Ocean. Our goal is to conduct a model-data comparison between time-series of surface radiocarbon from a suite of three-dimension ocean models that were included in the Ocean Carbon-Cycle Model Intercomparison Project 2 (OCMIP-2) and coral records from the coasts of Kenya and Sumatra (Fig. 1).

We begin by introducing coral radiocarbon as a tracer for water mass circulation and providing a brief description of model characteristics and the OCMIP-2 protocol for ^{14}C simulation (Section 2). Section 3 discusses intermodel differences with respect to the coral radiocarbon time-series at the Sumatra and Kenya sites and ranks the simulations in terms of model performance; next, we examine intrabasin surface radiocarbon differences across the equatorial Indian Ocean among the coral and model time-series. In addition, in this section we isolate features (e.g., model forcing or physics) related to model performance and evaluate parameterizations of lateral and vertical mixing schemes. The following section examines output from four sensitivity runs with one model. Finally, we summarize our findings (Section 4).

2. Background

2.1 Coral Radiocarbon as a Tracer for Water Mass Circulation

Corals incorporate dissolved inorganic carbon (DIC) from the surrounding seawater into their skeleton. As a result, coral $\Delta^{14}C$ reflects the seawater $^{14}C/^{12}C$ ratio at the time of precipitation**.** After correcting for decay from the time of formation until A.D. 1950 and for isotope fractionation (between ^{13}C and ^{12}C) by normalizing to a $\delta^{13}C_{PDB}$=-25 ‰ (Broecker and Olson, 1961), the accreted aragonite provides a record of $^{14}C/^{12}C$ ratios present in seawater (e.g., Druffel and Linick, 1978; Druffel, 1982; Druffel, 1989; Brown et al., 1993; Guilderson et al., 1998; Guilderson et al., 2000). Surface ocean ^{14}C levels can be determined for the past 100 years or more in many regions of the tropics and sub-tropics where corals grow. Radiocarbon in oceanic DIC is mainly controlled by changes in ocean circulation rather than by atmosphere exchange of CO_2 (Druffel and Suess, 1983). Furthermore, the residence time of surface mixed layer waters is much

shorter than the air-sea equilibration time (~10 yrs) such that $\Delta^{14}C$ in the mixed layer traces changes in circulation. Therefore, coral $\Delta^{14}C$ records have been used to infer past changes in surface-subsurface vertical mixing as well as horizontal current shifts (e.g., Druffel, 1997; Guilderson and Schrag, 1998; Guilderson et al., 1998; Druffel et al., 2001).

To document the temporal and spatial evolution of the ^{14}C gradient in the tropical Indian Ocean we use accelerator mass spectrometric (AMS) measurements of $\Delta^{14}C$ in *Porites* corals from Watamu, Kenya (3ºS, 39ºE; Grumet et al., 2002a,b) and the Mentawai Islands, Sumatra (0ºS, 98ºE; Grumet et al., 2004) (Fig. 1). Methods of $\Delta^{14}C$ calculation are described in Stuiver and Polach (1977). A 63 cm coral core was collected from massive hermatypic corals *Porites lutea* from Watamu, Kenya in August 1996. The Kenya coral site is approximately 600 m offshore and 200 m landward of an intermittent barrier system. Water depth at this collection site is about 7 m. At the Mentawai Islands, Sumatra site, a 2.7 m long core was collected in June 2001. The Sumatra collection site is approximately 400 m offshore of Penang Island (0º08'S, 98º31'E) in the northern section of the Mentawai Island chain. Petrographic analysis of thin sections from the coral cores showed the original coral aragonite to be well preserved. These two records comprise the first intrabasin record of surface water $\Delta^{14}C$ variability in the equatorial Indian Ocean and offer a basin wide view of equatorial thermocline dynamics and uptake of the bomb transient.

2.2 The Ocean Carbon-Cycle Model Intercomparison Project (OCMIP)

The OCMIP was initiated in 1995 by the International Geosphere-Biosphere Program (IGBP) and the Global Analysis, Interpretation and Modeling Task Force

(GAIM) to help identify and understand differences between three-dimensional ocean circulation/carbon-cycle models. A second phase of OCMIP was initiated in 1998 with 13 modeling groups and data specialists in inorganic carbon, radiocarbon and CFCs. The focus of OCMIP-2 is on simulation of the carbon cycle and anthropogenic CO_2 (Orr et al., 2001), CFCs (Dutay et al., 2002) and natural ^{14}C (Matsumoto et al., 2004).

Table 1 provides a list of OCMIP-2 models employed in this study and the principal model differences, including surface forcing and model architecture (e.g., grid size, horizontal and vertical resolution, topography). The SOC and PIUB models were omitted from this study because they do not meet 3-D requirements. While all models have global coverage, our work focuses on the equatorial Indian Ocean and our results and discussion are restricted to this region. The models are coarse resolution, primitive-equation models solving prognostically for the evolution of velocity, temperature and salinity in three dimensions. Exceptions are the Max Planck (MPIM) and Alfred Wegener (AWI) models; the former neglects non-linear terms in the advection equation (Maier-Reimer et al., 1993) and the latter uses an adjoint data assimilation techniques to derive circulation from hydrographic and geochemical data (Schlitzer, 1999). In a similar manner, IPSL restores subsurface temperature and salinity to climatological values. Four of the models (AWI, IGCR, IPSL, and MPIM) are offline, using pre-calculated, stored velocities to transport tracers (e.g., $\Delta^{14}C$). None of the models have horizontal resolution adequate to resolve eddies, and each model differs in their subgrid-scale parameterization of these eddies (Dutay et al., 2002; Doney et al., 2004). Other differences include dynamic forcing (e.g., heat flux, freshwater flux and wind stress), grid resolution, and topography, which can affect predicted circulation (Duffy et al., 2002. Wickett et al.,

2003). All modeling groups use a standard set of geochemical boundary conditions to facilitate model comparison (Najjar and Orr, 1999). In all models, the flux of radiocarbon at the air-sea interface was calculated according to OCMIP-2 protocol (http://www.ipsl.jussieu.fr/OCMIP). The modeling protocol does take into account the rising levels of CO_2 in the atmosphere and the increase in surface water DIC. Simulated fluxes vary from model to model because model temperature and salinity fields differ as well as prognostic model variables, such as temperature, salinity, DIC and alkalinity, which contribute to differences in air-sea CO_2 fluxes among the models.

The vertical mixing coefficients (K_v) and vertical coordinate scheme for each model in addition to the vertical resolution in the upper ocean are outlined in Table 1. Two of the models (CSIRO and MPIM) use vertical diffusion coefficients which depend on calculated vertical density gradients, while four of the models (IPSL, NERSC, NCAR and UL) use a relatively dynamic mixed layer parameterization. The remaining models have a prescribed profile of vertical eddy diffusion coefficients such that the vertical eddy diffusivity and viscosity are independent of time and space. The lateral, subgrid-scale mixing of tracers is parameterized using horizontal Laplacian diffusion in three models (IGCR, MPIM and UL) while the remaining models employ either a mixing scheme oriented along isopycnal surfaces, or a combination of isopycnal mixing and a parameterization to represent the effect of subgrid-scale eddies on the thickness and slope of isopycnal layers (Gent and McWilliams, 1990). The models are forced with monthly climatological physical data except for AWI and IGCR, which are forced with annual mean fields.

Initial conditions were obtained by running the models under a 0 per mil atmosphere until 98% of the ocean volume had a $\Delta^{14}C$ drift of less than 0.001 per mil/year. In terms of ^{14}C age, this is equivalent to a drift of 8.27 years per 1000 years of simulation (Aumont et al., 1998). For most models, these criteria can be reached only after integrating at least a few thousand model years. For the historical runs initial atmospheric $\Delta^{14}C$ concentrations for the period 1765-1995 were compiled from Enting et al. (1994) and Hessheimer et al. (1994). The NERSC model was the only participant that did not reach equilibrium during the pre-industrial period (Y. Gao, person. comm.).

Two-dimensional surface $\Delta^{14}C$ plots from the pre-bomb period were used to asses the spatial variability. In some cases site specific surface $\Delta^{14}C$ values were biased towards elevated model $\Delta^{14}C$ surface values in the eastern basin from the Indonesian Through flow (ITF), and depleted model $\Delta^{14}C$ surface values in the western basin from the upwelling regions of Somalia and Oman. As a result of unique dynamical processes acting in these regions (e.g., subduction, coastal upwelling, etc.) there is sufficient spatial variability in bomb produced tracer distribution. This is confirmed by additional ^{14}C studies (Broecker et al., 1985; Bard et al., 1989; Bhushan et al., 1994; 2000; Ostlund and Grall, 1991; Somayajulu et al., 1999). Grumet et al. (2002b) showed that Kenya $\Delta^{14}C$ values agreed well with surface observations from nearby GEOSECS and INDIGO stations, suggesting that there is no delay in the surface observations and coral data. However, the GEOSECS and JADE hydrographic stations, 439-442 and 12-16, respectively, are not appropriate analogs for the Sumatra coral data. These stations indicate relatively higher surface $\Delta^{14}C$ values compared to the coral $\Delta^{14}C$ values by approximately +20‰. These sites are more likely to be bathed in waters from the

Indonesian Throughflow (ITF) since the majority of ITF transport is between 7º and 15ºS (Fieux et al., 1994; Wijffels et al., 2002). The invasion of water from the Pacific Ocean is apparent in isotopic tracers as a maximum input of bomb produced ^{14}C, tritium and strontium (e.g., Fine 1985; Bard et al, 1988; Toggweiler and Trumbore, 1985). Likewise, Grumet et al. (2004) compared pre-bomb $\Delta^{14}C$ values from biogenic archives in the surrounding Indian Ocean (Dutta et al., 2001; Bhushan et al., 1994; Southon et al., 2002) to conclude that the Indonesian Seas, Bay of Bengal and Arabian Sea were not source regions for ^{14}C-depleted water to the coast of Sumatra. Instead, the coral $\Delta^{14}C$ record captures ^{14}C-depleted water derived from upwelling along the coast of Java and Sumatra. To avoid potential bias associated with the use of different and model-specific grid points, simulated $\Delta^{14}C$ time-series and vertical profiles were obtained from the four closest grid points (i.e., closest to the coral sites). Each grid cell was weighted by the product of its area and the inverse of its distance from the respective coral site. This approach assumes that surface $\Delta^{14}C$ values from the corals and model grid points adequately capture adjacent ocean conditions. We investigated this assumption and the corals' sensitivity to adjacent open ocean conditions by comparing monthly coral oxygen isotope ($\delta^{18}O$) data at each site to GOSTA GISST 2.2 instrumental SST data (Rayner et al., 1996). The ratio of ^{18}O to ^{16}O ($\delta^{18}O$) in biogenic carbonates such as corals primarily reflects sea surface temperature (SST) with a secondary influence from precipitation/evaporation changes and has been used to reconstruct past variability in SST and salinity (e.g., Charles et al., 1997; McCulloch 1999; Swart et al., 1999; Cole et al. 2000). A comparison of monthly instrumental SST data from an area between 10^oN-10^oS and 39^oE-59^oE to the Kenya monthly $\delta^{18}O$ data yields a correlation coefficient of -0.70

(n=571) from 1947 to 1994. In a similar manner, a comparison of monthly instrumental data from an area between 10°N-10°S and 78°E-98°E to the Sumatra monthly $\delta^{18}O$ data yields a correlation coefficient of -0.51 (n=526) from 1947 to 1990. The correlation at both sites becomes stronger during the most recent 20 years as uncertainties derived from ship observations are reduced in the instrumental record. These correlation coefficients, despite uncertainties in the ship observations and minor chronologic offsets, suggest that adjacent SSTs are being captured in the coral $\delta^{18}O$ records. Thus, given the correlation of the coral $\delta^{18}O$ data to instrumental SST data, as well as the relationship between the coral $\Delta^{14}C$ data to hydrographic surface water $\Delta^{14}C$ data (as discussed above), we are confident that the coral geochemistry sufficiently represents adjacent open ocean conditions.

3. Results and Discussion

Since the corals were growing at depths (between 3 to 7 m) that are well within the surface layer of every model, we compared coral $\Delta^{14}C$ values to simulated surface level values in each model (Tbl. 1). From 1900 to 1954 the models indicate a drift of -9.7‰ and -10.8‰ at the Kenya and Sumatra sites, respectively. The lowering of atmospheric $\Delta^{14}C$ to negative values prior to the 1950s as a result of fossil fuel burning is referred to as the Suess effect (Stuiver and Quay, 1981). The model simulation of the Suess effect off the coast of Kenya is in agreement with a coral estimate of approximately -10‰ (Grumet et al., 2002a,b). However, coral studies from the coast of Sumatra indicate that the Suess effect at this site is negligible (less than 2‰) since mixing of deeper, ^{14}C-depleted water in the eastern Indian Ocean dilutes the fossil fuel signal during the pre-nuclear period (Grumet et al., 2004). The coral records indicate a zonal gradient

in surface $\Delta^{14}C$ values during the pre-bomb period (Grumet et al., 2004). A zonal section of radiocarbon values in the upper 1000m across the WOCE I2 section (~8°S) captures this zonal gradient in the upper 1 km (Key and Quay, 2002). As revealed in bomb ^{14}C zonal cross sections from Indian Ocean gridded WOCE data, ^{14}C isolines are depressed in the west compared to relatively flat isolines that slope towards the east (http://cdiac.ornl.gov). The influence of deeper, ^{14}C-depleted water in the eastern Indian Ocean relative to the western Indian Ocean is also seen in sections of anthropogenic CO_2 along 57ºE and 92ºE (Sabine et al., 1999). Compression and shoaling of isopycnal surfaces along 92ºE facilitates mixing of deeper, ^{14}C-depleted water in the eastern Indian Ocean. For the remaining portion of the discussion, we have not applied a fossil fuel correction since the atmospheric $\Delta^{14}C$ forcing for both the models and observations contain a Suess effect, and because the dilution due to burning of fossil fuels is insignificant compared to the ^{14}C enrichment from nuclear weapons testing in the 1950s.

3.1 Pre-bomb period and timing of bomb-induced maximum

Simulated pre-bomb global average surface values, calculated as the global mean from 1948 to 1954, range from -36‰ (NERSC) to -62‰ (AWI) and yield a standard deviation of ±7‰. The range of model pre-bomb values at each site, calculated as the mean from 1948 to 1954 is slightly greater than the inter-model range of global-mean values (Fig. 2). The former values range from -34‰ (NERSC) to -90‰ (NCAR) at Sumatra with a standard deviation of ±16‰, and range from -32‰ (NERSC) to -65‰ (NCAR) with a standard deviation of ±10.2‰ at Kenya (Fig. 2). At each site, the pre-bomb annual mean values correlate with global mean values (r^2=0.83 and 0.64, p=0.05, Kenya and Sumatra respectively; Fig. 2), suggesting that biases accrued during the

equilibrium runs affect the site specific and global pre-bomb averages in a similar manner.

Surface ocean radiocarbon time-series from each model reflect the record of anthropogenic input of ^{14}C into the atmosphere from nuclear weapons as well as the dilution by burning fossil fuels during the industrial revolution (Fig. 3). At both sites post-bomb coral $\Delta^{14}C$ peaks during the mid-1970s (Fig. 4), almost a decade after the 1963 atmospheric bomb radiocarbon peak, reflecting the time required for the surface ocean to equilibrate with the atmosphere with respect to $\Delta^{14}C$ (Nydal, 2000). In comparison, the models show surface ocean maxima in $\Delta^{14}C$ as early as 1968 (MIT) and as late as 1980 (CSIRO) at Sumatra, and as early as 1971 (MPIM) and as a late as 1981 (AWI) at Kenya (Fig. 4). The general inability of models to simulate the timing of the bomb ^{14}C maximum in the Indian Ocean is one of our key findings.

Clearly, extrema stand out among the various models as seen in the large range of model simulated amplitude ($\Delta\Delta^{14}C$) of $\Delta^{14}C$ and the timing of the post-bomb maximum (Fig. 4). The performance of each model was measured by calculating its root mean square (RMS) difference with respect to observed ^{14}C values. As seen in Fig. 5, several models are outliers, NERSC, AWI, NCAR and MPIM with the remaining models clustered towards lower RMS difference. The NERSC model overestimates surface $\Delta^{14}C$ at both sites, while the AWI underestimate surface values. The NCAR model underestimates surface $\Delta^{14}C$ values at the Sumatra site and MPIM model overestimates surface $\Delta^{14}C$ values at Kenya. These results are discussed in more detail below. However, we first examine the models' ability to capture the zonal gradient in $\Delta^{14}C$ across the equatorial Indian Ocean as captured in the coral and hydrographic data.

3.2 Intrabasin Comparison

The Kenya $\Delta^{14}C$ response leads the Sumatra response during the initial input of bomb ^{14}C by 2-3 years between 1954 and 1968 (Fig. 6). This relationship is also shown in Figure 5b when the difference between the Kenya and Sumatra records is positive. The post-bomb recovery appears to be slightly faster at the Sumatra site, as illustrated when the difference between the two sites is once again positive. However, between 1968 and 1977 the Sumatra response exceeds the Kenya response and the difference between the two sites is negative.

Kenya coral $\Delta^{14}C$ values rise quickly because surface waters are in prolonged contact with the atmosphere and are influenced by lateral advection of surface water along the coast of east Africa (Grumet et al., 2002b). The absence of a distinct subannual $\Delta^{14}C$ signal during the pre-bomb period suggests that open and coastal upwelling is negligible off the coast of Kenya (Grumet et al., 2002a). At sites such as Kenya, surface radiocarbon values tend to rise more quickly where there is greater influence of horizontal transport of water and very little upwelling (Druffel, 1996). In contrast, at Sumatra where there is greater exchange between the surface and subsurface waters due to wind-induced upwelling and rapid convective mixing, there is subsequent storage of bomb radiocarbon in the upper few hundred meters of the water column. As mentioned earlier, compression and shoaling of $\Delta^{14}C$ isolines facilitates mixing of deeper, ^{14}C-depleted water in the eastern Indian Ocean. In turn, these processes dilute the effect of the uptake of bomb produced ^{14}C by the surface-ocean and surface $\Delta^{14}C$ values at Sumatra are delayed relative to those at Kenya. (Grumet et al., 2004).

The models do not capture the initial lead in bomb response observed in the Kenya coral record, as seen in Figure 7 when the difference between the models simulation at the two sites is either close to zero or negative until the late 1960s. Rapid mixing between the surface and subsurface along the coast of Sumatra can also explain differences in the pre-bomb averages between the Kenya and Sumatran coral sites. The decrease in Sumatra pre-bomb average from 1877 to 1954 is less than 2‰, which is barely distinguishable from the calculated standard error of ~1‰ (Grumet et al., 2004). These results indicate a minimal Suess effect at the Sumatra site. In contrast, Grumet et al. (2002b) applied a 10‰ Suess correction to the Kenya pre-bomb $\Delta^{14}C$ record. Applying this correction yields a Kenya pre-bomb average of -50‰, while the Sumatra pre-bomb record exhibits a more depleted pre-bomb average, -64‰. Assuming appropriate Suess corrections have been applied at both sites, pre-bomb ^{14}C values are offset by almost 14‰ across the equatorial Indian Ocean. According to a simple box model, a vertical water mass mixing rate (e.g., mixing of surface and subsurface waters) of 2-3 years at Sumatra is required in order to satisfy the pre-bomb steady state conditions at the two sites (Grumet et al., 2004). This was sufficient for satisfying the pre-bomb steady state conditions since there is no vertical mixing at Kenya. Results of the forward model calculation illustrate that this vertical water mass mixing rate at Sumatra can help explain the 2-3 year lag in Sumatra $\Delta^{14}C$ during the during the maximum input of bomb-produced ^{14}C (Grumet et al., 2004). Thus, a second major finding of this study is that the models are not able to capture an appropriate vertical water mass mixing rate at the Sumatra site.

In their assessment of model performance with the OCMIP-1 models, Orr et al. (2001) point out that the simulations have difficulty representing shoaling of the mixed layer with too much mixing in the west and too little mixing in the east. However, in our study eight out of eleven models are able to capture enriched surface $\Delta^{14}C$ values at the Sumatra site, suggesting that the OCMIP-2 participants have improved their ability to capture the east-west surface ^{14}C gradient, albeit with faster response at Sumatra relative to the coral record. The exceptions to this behavior are the simulations from the NCAR, MPIM and CSIRO models. In these three models, the Kenya response is consistently elevated relative to the Sumatra site, as indicated by positive values throughout the time-series (Fig. 7). Thus, these models in the second phase of OCMIP still have difficulty simulating shoaling of the mixed layer.

3.3 Sensitivity to Treatments of Lateral Subgrid Scale Mixing

One of the major objectives of this study is to investigate the sensitivity of model performance to treatments of lateral subgrid scale mixing. The models that incorporate a horizontal subgrid lateral-mixing scheme are the IGCR, MPIM and UL models. As seen in Fig. 5, the RMS difference of the MPIM simulation indicates that for this set of solutions, the MPIM is an outlier. As seen in the time-series plots (Fig. 3), the MPIM model maximum is earlier than the coral data and the recovery is faster than the observed data at Sumatra. At the Kenyan site, this model overestimates surface $\Delta^{14}C$ values by almost 50‰. As a result, the RMS difference is elevated, especially at the Kenya site. In comparison, UL and IGCR models are able to simulate the coral time-series but with slightly depleted $\Delta^{14}C$ amplitudes (Fig. 4). Therefore, model simulation based on the horizontal subgrid lateral-mixing scheme is not an indication of model performance.

The second group of lateral subgrid scale mixing scheme is represent by the AWI and NERSC models, which employ an isopycnal subgrid lateral-mixing scheme. Isopycnal mixing schemes help eliminate nonphysical diapycnal mixing associated with horizontal diffusion schemes (e.g., England and Rahmstorf, 1999), referred to as the Veronis effect (Veronis, 1973; Toggweiler et al., 1989). Both of these models have a large RMS difference and were not able to simulate surface $\Delta^{14}C$ values at either the Sumatra or Kenya site. As shown in Figure 3, the AWI simulation underestimates surface $\Delta^{14}C$ values, while the NERSC model overestimates surface $\Delta^{14}C$ values. As a group, these models with a lateral subgrid scale mixing scheme did not perform well. Furthermore, based on this set of solutions compared to those simulations from models with a horizontal subgrid lateral-mixing scheme, there is no indication that spurious upwelling is sensitive to the treatment of lateral subgrid scale mixing (e.g., horizontal versus isopycnal mixing) along the coasts of Kenya and Sumatra.

The third group of models, which include the CSIRO, IPSL, MIT, NCAR, PRINCE, and LLNL models, employ an isopycnal subgrid lateral mixing scheme combined with the Gent McWilliams (GM) eddy parameterization (Gent and McWilliams, 1990). Except for the NCAR model, this group of models shows a clustering of relatively reduced RMS difference in Figure 5. At the Kenyan site, this group of numerical models is able to simulate the coral $\Delta^{14}C$ time-series relatively well (Fig. 3a). Within in this group, there is a larger spread of model simulation surface $\Delta^{14}C$ at the Sumatra site compared to Kenya (Fig. 3b and 5). Despite the improvements from GM, the thermocline in the Indo-Pacific basin is generally too diffuse in OCGMs in the Pacific Ocean. (Guilderson et al., 2000; Rodgers et al., 2000). Thus, this may contribute

to the difficulty of modeling $\Delta^{14}C$ uptake and distribution, especially in the eastern Indian Ocean. Furthermore, the incorporation of GM may be more important at higher latitudes (Duffy et al., 1995b).

Within this group, the IPSL model does the best job simulating the observed coral $\Delta^{14}C$ time-series at both sites. However, IPSL is the only model to restore subsurface temperature and salinity to climatological values to assure that the geostrophic circulation in the model approaches that observed in the real ocean (Aumont et al., 1999; Orr, 2002). This is similar to the adjoint method used in the AWI model in the sense that both models' circulations are strongly influenced by observations. The strong performance from the IPSL may be attributed to the use of subsurface restoring or to higher resolution in the equatorial region. A key finding from this study is that altogether we find little evidence that ability to simulate surface-ocean ^{14}C in the Indian Ocean is strongly sensitive to choice of lateral mixing scheme with the exception that GM may be helpful at the Kenya site. In a similar manner, Gnanadesikan et al. (2002) found that new production in the Atlantic Ocean was only weakly sensitive to the level of lateral diffusion.

3.4 Sensitivity to Vertical Mixing Schemes

A second major objective of this study is to evaluate the sensitivity of model performance to treatments of vertical mixing schemes. The vertical mixing coefficients (K_v) for each model are outlined in Table 1. The first group of models, represented by AWI, IGCR, LLNL, MIT, and PRINCE, assume an implicit mixed layer of fixed depth and vertical mixing occurs via diffusion and convective instability. The second group of models, which include CSIRO and MPIM, use vertical diffusion coefficients which

depend on calculated vertical density gradients. The third group of models, which is comprised of the IPSL, UL, NCAR, and NERSC models, include a sophisticated mixed layer treatment. With a sophisticated mixed layer treatment, the external forcing is applied, the boundary layer depth is determined, and profiles of diffusivity and viscosity are formulated (Large et al., 1994). The purpose of these schemes is to allow the simulated mixed layer depth and rates of interior ocean mixing to depend on the surface forcing and local conditions, such as the vertical density gradient. The IPSL, NERSC, and UL models employ the Turbulent Kinetic Energy (TKE) closure scheme (Blanke and Delecluse, 1991; Gaspar et al., 1990), while the NCAR model employs the non-local boundary layer parameterization, K Profile Parameterizations (KPP) (Large et al., 1994; 1997). The KPP mixing scheme is designed to represent both convective and wind-driven entrainment by determining the profiles of vertical viscosity, vertical tracer diffusivity, and non-local boundary layer tracer transport (Large et al., 1997). In comparison, the TKE mixing scheme provides realistic simulations of the vertical turbulent mixing by solving the turbulent kinetic energy equation; mixed layer dynamics are computed from heat fluxes and wind stress at the surface. The eddy viscosity and diffusivity are defined as the product of the root square of the turbulent kinetic energy and a mixing length (Blanke and Delecluse, 1992; Gaspar et al., 1990).

As already discussed, the NCAR simulation drastically underestimates the surface $\Delta^{14}C$ values at the coast of Sumatra (Fig. 3b and 4b). This may be due to overly-rapid vertical mixing. Dutay et al. (2002) also found that incorporating KPP did not help simulated penetration of CFC-11 into the subsurface layers, where the NCAR model has a weaker vertical penetration than the Princeton model which has no mixed-layer model.

In comparison, the NERSC model overestimates the $\Delta^{14}C$ peak values at both sites (Fig. 3 and 4). The NERSC model is the only participant to utilize an isopycnal vertical coordinate scheme (versus a z-coordinate scheme employed by the remaining models) where the vertical coordinate is divided into a series of discrete layers each of uniform density that vary in time and space (Orr, 2002). In this configuration, the mixed layer depth appears to be too shallow and $\Delta^{14}C$ values remain elevated throughout the water column (Fig. 8a,b). The annual mean temperature profile from the NERSC model supports this notion by illustrating a larger degree of stratification in the upper 100 m and relatively colder temperatures below 50 m (Fig. 9a,b). A shallow mixed layer facilitates the accumulation of bomb ^{14}C in the surface layer. We also found evidence of a shallow mixed layer when we compared the NERSC simulated meridional $\Delta^{14}C$ depth profiles along the Sumatra coast to the WOCE hydrographic meridional $\Delta^{14}C$ depth profiles. Therefore, while previous studies have shown that OGCMs that embed a dynamic mixing scheme (e.g., TKE or KPP) better represent SST and the vertical mixed layer structure (Gaspar et al., 1990; Large et al., 1997; Goosse et al., 1999), these dynamic mixed layer schemes provide additional degrees of model freedom, and thus can exhibit greater sensitivity to inappropriate physical forcing. A key conclusion of this study is that while this group of models is capable of producing better results, they can also produce anomalous results, as illustrated by the NCAR and NERSC models as shown in Figure 5.

The second group of models, CSIRO and MPIM, use vertical diffusion coefficients which depend on calculated vertical density gradients. At the Kenya site, the CSIRO simulation is within the constraints provided by the coral data (Fig. 3a and 4a). However at Sumatra, the CSIRO model exhibits a delayed response and underestimates

the $\Delta^{14}C$ amplitude (Fig. 4b). The sea-surface temperature at this site is colder relative to the average simulated sea-surface temperature (Fig. 9b). Therefore, vertical mixing appears to be overly active at this Sumatra such that colder, depleted ^{14}C water is brought up from depth to the surface layer. Within this same group of models, In contrast, at the Kenya site, the MPIM model overestimates the amplitude of $\Delta^{14}C$ (Fig. 4a) and the recovery of this model is relatively fast at both sites (Fig. 3). The MPIM pre-bomb vertical $\Delta^{14}C$ gradient (normalized to the coral surface $\Delta^{14}C$ value at each site) in the upper 160 m is also the greatest (Fig. 8b). The temperature profile shows a similar gradient in the upper 100 m as well. This strong stratification may play a role in inhibiting vertical mixing and vertical penetration of the transient radiocarbon tracer. Because the vertical diffusivity coefficient is dependent on stratification (Tbl. 1) (Maier-Reimer person. comm.), greater stratification is intimately linked to a lower vertical mixing coefficient in the upper water column and to a higher surface $\Delta^{14}C$ value. This can lead to feedback between mixing rate and stratification. All this suggests that near-surface vertical mixing is too slow in the MPIM model and may reflect the choice of vertical mixing scheme or the fact that this model neglects non-linear terms in the advection equation. In either case, as shown in Figure 5, the MPIM remains an outlier while within this same group the CSIRO model exhibits a smaller RMS difference.

The remaining group of models, consisting of the AWI, IGCR, MIT, and PRINCE models, has a prescribed profile of vertical eddy diffusion coefficients such that the vertical eddy diffusivity and viscosity are independent of time and space. The vertical mixing coefficient varies between 0.1 to 0.2 cm^2/s (Tbl. 1). The LLNL model uses a prescribed K_v that varies with depth, K_v is 1 cm^2/s at 25 m and 0.2 cm^2/s at the base of the

mixed layer. Within this group, the AWI simulation the model has the largest RMS difference (Fig. 5). As mentioned earlier, the AWI model underestimates the $\Delta\Delta^{14}C$ at both sites (Fig. 3 and 4). The AWI model uses the adjoint data assimilation techniques in which hydrographic and geochemical data are used to drive circulation in order to minimize the model-data misfit for temperature, salinity, oxygen, nutrients and inorganic carbon (Schlitzer, 1999; 2002). Unlike dynamical models that use approximations of the momentum equation and external forcing at the sea-surface to calculate time-varying circulation, the AWI model has an annually-averaged 3-D flow field obtained by assimilating available historical hydrographic data. There are temperature offsets in the AWI model relative to Levitus since the former derives temperature from individual hydrographic sections that frequently deviate from Levitus climatology (Doney et al., 2004). This is apparent in the vertical temperature profiles at both sites (Fig. 9). Anomalously cold near surface temperatures derived from hydrographic sections near the coasts of Kenya and Sumatra may be indicative of over simulating vertical mixing in the AWI model. The inability of the AWI model to explicitly model summer time stratification and wintertime deep convection together with the small mixing coefficients is also believed to be responsible for relatively patchy field of air-sea fluxes found in CFC simulations (Weirig in Orr, 2002). Thus, errors in the simulated hydrographic properties may indicate circulation problems with the AWI set of solutions that are relevant to the simulated tracer field of interest, in this case $\Delta^{14}C$. Disregarding the AWI simulation however, any limitation associated with a prescribed profile of vertical eddy diffusion coefficients does not seem to hinder the performance of this group of model simulations. Therefore, we conclude that simulations from this group of models are as

equally acceptable to those with either a vertical diffusion coefficient dependent on calculated vertical density gradients or a sophisticated mixed layer treatment.

3.5 Sensitivity to additional factors

The offline models (AWI, IGCR, IPSL, and MPIM) do not solve the momentum equations for each time step but instead use stored pre-calculated velocities to transport tracers (e.g., $\Delta^{14}C$). In principle, this has little effect on simulated tracer distribution. At the Kenyan site, the AWI model has the smallest $\Delta\Delta^{14}C$ while the MPIM model exhibits the largest $\Delta\Delta^{14}C$ (Fig. 4), despite the commonality of both being offline models. In contrast, the IPSL model has the smallest RMS difference even in comparison to the online models; the IGCR $\Delta\Delta^{14}C$ is slightly depleted relative to the observed data (Fig. 4). At the Sumatra site, the offline models either exhibit a smaller $\Delta\Delta^{14}C$ (AWI and IGCR), peaks earlier (MPIM) or is comparable (IPSL) to the coral time-series (Fig. 4). There is no common behavior among the online models in terms of their $\Delta^{14}C$ simulation, as seen in the scatter of RMS difference in Figure 5. Thus, as should be true, whether a model is online or offline is not a determinant factor in how well the model predicts surface ocean $\Delta^{14}C$ variability off the coasts of Kenya and Sumatra.

Lastly, we examined how well the non-primitive equation models (AWI and MPIM) performed. The AWI model has the smallest $\Delta\Delta^{14}C$ at the Kenya site while the MPIM model exhibits the largest $\Delta\Delta^{14}C$ (Fig. 4). At the Sumatran site, the AWI response is smaller relative to the primitive equation models, while the MPIM $\Delta^{14}C$ response is similar to the coral time series (Fig. 4). For these particular observations the models are not sensitive to approximation of horizontal momentum equation. In summary,

3.6 Sensitivity Tests

In order investigate sensitivity to representation of the mixed layer, we ran four separate runs with the LLNL model, a variant of the GFDL MOM 1.1. The runs include isopycnal mixing scheme and the GM eddy parameterization. In comparison to the LLNL model used in OCMIP-2, forcing for the sensitivity runs was climatology calculated from NCEP reanalysis data for momentum (i.e. wind); heat fluxes were calculated from bulk formulae and salinity was restored to Levitus surface observations except under sea ice. The tracer time step was 1 day and the momentum time step was 1 hour.

Run 0 included the KPP mixed layer model (Large et al., 1994; 1997) and a calculated vertical mixing coefficient in the ocean interior whose value is proportional to 1/N where N= the local Brunt Vailasa frequency (a measure of the water column stability in the main thermocline and reflects resistance to vertical displacement of water parcels). Run 1 included KPP and a specified interior mixing coefficient which is uniform in space and time. Run 2 excluded KPP, and included a specified interior mixing coefficient and a 50 m mixed layer depth. Run 3 excluded KPP, and included a specified interior mixing coefficient and a 25 m mixed layer depth.

At the Kenya site, runs 2 and 3 represent the end members with run 2 underestimating the $\Delta^{14}C$ surface levels and run 3 overestimating the $\Delta^{14}C$ surface levels, suggesting that the true mixed layer depth varies between 25 to 50 m off the coast of Kenya (Fig. 10a). Runs 0 and 1, which included KPP, are very similar to one another, suggesting that changes in surface $\Delta^{14}C$ values are relatively insensitive to interior mixing rates. These runs exhibit a post-bomb peak earlier than the coral time-series and demonstrate a faster recovery period. Previous work suggests that the reduced seasonal

amplitude in the Kenya $\Delta^{14}C$ time-series reflects mixing with a "younger" undercurrent (Grumet et al. 2002b; 2004). In other words, as the bomb $\Delta^{14}C$ signal penetrates the upper water column, the oceanic $\Delta^{14}C$ maximum is below the surface. This pattern is observed in 1995 WOCE data that show upwelled waters at low latitudes in the Pacific having higher bomb radiocarbon levels than during the 1978 GEOSECS survey (Key, 1997). The delayed post-bomb peak in the coral record relative to the model suggests that sufficient time has elapsed to allow mixing between the surface and subsurface to compete with air-sea exchange processes in determining the surface ocean $\Delta^{14}C$ signature in the western Indian Ocean (Grumet et al., 2002b). However, for various reasons (e.g., coarse resolution, inappropriate physical forcing, etc.) the model is unable to properly simulate this mixing with bomb-laden subsurface water.

The four separate sensitivity runs at the Sumatra site are very similar to each other and to the coral time-series (Fig. 10b), which suggests that increasing the mixed layer depth from 25 to 50 m does not reduce the surface $\Delta^{14}C$ concentration. The insensitivity to mixed layer depth may be explained by active convective adjustment (i.e., downwelling) at Sumatra such that mixing between the various levels is rapid and the effective mixed layer depth is essentially the depth of convection. The downwelling captured by the models helps explain the mixing down and subsequent storage of bomb radiocarbon off the coast of Sumatra and the delay relative to the Kenya record.

As shown with previous studies, coastal processes such as convective mixing and lateral advection are important factors in determining the temporal evolution of surface $\Delta^{14}C$ in the Indian Ocean Grumet et al. (2002b; 2004). Using the GFDL MOM 3, Gnanadesikan et al. (2002) found convection to be a key component in

supplying nutrients to the surface ocean. Convection can lead to rapid mixing and as well as subsurface ^{14}C enrichment. As demonstrated by the sensitivity runs with the LLNL model and the OCMIP-2 comparisons discussed above, these coastal processes are not adequately captured by coarse resolution models which are better suited for large scale circulation. The success of a simple upwelling-diffusion (UD) model to match measured bomb ^{14}C in the mixed layer by Jain et al. (1995) however is encouraging. Thus, this type of model-data comparison should be done with a suite of UD models.

4. Conclusion

We evaluate the ability of a group of ocean models to simulate the time-series of surface ocean ^{14}C in the Indian Ocean during the influx of bomb produced ^{14}C. There is considerable variation of simulated $\Delta^{14}C$ outside the constraints provided by the coral $\Delta^{14}C$ time-series. The models with the greatest RMS difference are the AWI, MPIM, NERSC and NCAR simulations, indicating that for this set of solutions these models can not capture the temporal evolution of surface $\Delta^{14}C$ on either side of the equatorial Indian Ocean. In contrast, the IPSL and UL simulations most closely matched the coral time-series, suggesting that models that incorporate a dynamic vertical mixing scheme may be capable of producing better simulations. However, within the same group of numerical models there is a large degree of variation, as demonstrated by the NCAR and NERSC simulations which also employ a dynamic vertical mixing scheme, KPP and TKE respectively. Likewise, there is a large range of model performance between models with different lateral scale subgrid scale mixing. Thus, our key finding is that at both sites factors such as resolution, topography, physical forcing and horizontal advection are more important than mixing parameterization in explaining intermodel differences for

these simulations from 11 OCMIP-2 models. Another key finding is that the models are unable to simulate the intrabasin differences in surface $\Delta^{14}C$ captured in the Kenya and Sumatra coral $\Delta^{14}C$ time-series which may reflect the models' failure to simulate an appropriate vertical water mass mixing rate of 2-3 years off the coast of Sumatra. In addition, Follows and Marshall (1996) found that models which explicitly resolve geostrophic eddies can reproduce the longitudinal gradient in column inventories found in observational data. Based on their findings, eddy transfer of bomb $\Delta^{14}C$, which is not captured parametrically in the coarse resolution models, may be an important component in simulating the zonal $\Delta^{14}C$ gradient in the Indian Ocean.

There are large variations among the OCMIP-2 models in standard physical metrics (e.g., hydrographic fields, seasonal SST, mixed layer depth, etc.), some well outside the observational constraints. As Doney et al. (2004) conclude, errors in the physical metrics signify problems in the model representations of ocean transport and dynamics, problems that directly propagate into the OCMIP-2 preidcted ocean tracer variables. This is highlighted in the inadequate simulation of $\Delta^{14}C$ and CFC-11 inventories from a suite of 19 ocean carbon cycle models (Matsumoto et al., 2004). Given the wide range of hydrographic metrics, Doney et al. (2004) suggest that the OCMIP-2 analysis refocus on models deemed acceptable by a set of joint physical and transient tracer criteria based on observable fields, such as radiocarbon and CFC. This might reduce uncertainties in simulations of future anthropogenic CO_2 uptake.

Given the high degree of complexity within these OCMIP-2 models, it is difficult to attribute a single process that is responsible for poor model performance and to provide a remedy for model performance. However, because we found that within the same group

of numerical models there is a large degree of variation, an important conclusion and recommendation from this study is that the modeling community should focus on how well the standard physical metrics (e.g., hydrographic fields, seasonal SST, mixed layer depth, etc.) match the observational constraints rather than how well the models parameterize mixing.

How well the models simulate the rate and magnitude of recovery from the bomb perturbation will become increasingly more important as the ocean circulation has time to dissipate prior discontinuities between the two tracers since the relationship bomb ^{14}C and anthropogenic CO_2 is believed to become more linear with time. For example, in an OCMIP study, Orr et al. (2001) found that the relationship between Atlantic Ocean inventories of bomb ^{14}C and anthropogenic CO_2 was more linear when 1990 bomb ^{14}C inventories were employed instead of those from GEOSECS. There is still debate on the role of the coastal ocean on the carbon cycle. Therefore, in order to evaluate the temporal evolution of transient tracers there is an obvious need to develop regional high-resolution numerical models that can accurately capture coastal processes. Although our results are primarily qualitative and descriptive, we hope our efforts will stimulate modeling groups to continue sensitivity and model-data comparison studies to improve model performance, especially those aimed at representing dynamical processes responsible for surface ocean $\Delta^{14}C$ variability.

Acknowledgements

This work was supported by a U.S. D.O.E. Global Change Education Program Fellowship to N.S. Grumet. The sensitivity mixing experiments were funded under 01-ERI-009 for T. Guilderson and K. Caldeira. We thank two anonymous reviewers and the associate editor for their helpful comments and discussion in improving the manuscript.

This work was performed under the auspices of the U.S. Department of Energy by University of California, Lawrence Livermore National Laboratory under contract W-7405-Eng-48.

Figure Captions

Figure 1 Site map of coral sites off the coast of Kenya (3ºS, 39ºE) and coast of Sumatra (0, 98ºE) are designated as asterisks. The Indonesian Throughflow (ITF) transport, between 7º and 15ºS is indicated by arrows. The location of the INDIGO (squares) and GEOSECS (triangles) hydrographic stations used for comparison between coral and cruise surface $\Delta^{14}C$ are shown as well.

Figure 2 Model global pre-bomb vs. site specific pre-bomb $\Delta^{14}C$ (per mil) average values at the Kenya (A) and Sumatra (B) coral sites, both calculated as the mean from 1948 to 1954. Models are assigned a symbol according to the type of lateral mixing used in the simulation, horizontal models (squares), isopycnal models (crosses) and isopycnal plus Gent McWilliams (GM) eddy parameterization (triangles).

Figure 3 Model and coral $\Delta^{14}C$ (per mil) time-series centered at the (A) Kenya ($3^{o}S$, $39^{o}E$) and (B) Sumatra (0, $98^{o}E$) coral sites. Surface $\Delta^{14}C$ values from appropriate hydrographic sites (1986 INDIGO and 1978 GEOSECS surveys) near the Kenya site are shown for comparison. No appropriate coastal sites were available for comparison at the Sumatra site.

Figure 4 Amplitude of $\Delta^{14}C$ response (per mil) to bomb perturbation ($\Delta\Delta^{14}C$) vs. the peak year (defined as when the first derivative ($\Delta^{14}C/\delta t$) of the simulated response changes sign) compared to the (A) Kenya and (B) Sumatra coral data. Models are assigned a symbol according to the type of lateral mixing used in the simulation, horizontal models (squares), isopycnal models (crosses) and isopycnal plus Gent McWilliams (GM) eddy parameterization (triangles).

Figure 5 Root mean square (RMS) error between the OCMIP-2 models and the Kenya (x-axis) and Sumatra (y-axis) coral $\Delta^{14}C$ time-series. Models are assigned a symbol according to the type of lateral mixing used in the simulations and are designated as follows: horizontal models (squares), isopycnal models (crosses) and isopycnal plus Gent McWilliams (GM) eddy parameterization (triangles).

Figure 6 Intrabasin comparison between the annual Kenya and Sumatra coral $\Delta^{14}C$ (per mil) time-series. The time-lag in the Sumatra coral record represents a vertical water mass mixing rate of between 2-3 years at the Sumatra site (Grumet et al., 2004).

Figure 7 Longitudinal gradient in surface Δ14C values (per mil) across the equatorial Indian Ocean, calculated as the difference between annual Kenya and Sumatra $\Delta^{14}C$ values as shown here for both the coral and OCMIP-2 simulations.

Figure 8 Pre-bomb average $\Delta^{14}C$ (per mil) vertical profiles for the OCMIP-2 simulations in the (A) upper 1000 m at the Kenya site and (B) upper 160 m normalized to the Kenya pre-bomb $\Delta^{14}C$ average (-61 per mil).

Figure 9 Model climatological vertical temperature (^{o}C) profiles at the (A) Kenya and (B) Sumatra coral sites, as well as Levitus94 annual climatological vertical temperature profile (Levitus and Boyer, 1994).

Figure 10 Comparison of (A) Kenya and (B) Sumatra coral Δ^{14}C time-series to four sensitivity runs with the LLNL model, a variant of the GFDL

References:

Aumont, O., J.C. Orr, D. Jamous, P. Monfray, O. Marti, and G. Madec, A degradation approach to accelerate simulations to steady-state in a 3-D tracer transport model of the global ocean, *Clim. Dyn., 14*, 101-116, 1998.

Bard, E., M. Arnold, J. R. Toggweiler, P. Maurice and J. C. Duplessy, Bomb C-14 in the Indian-Ocean measured by accelerator mass-spectrometry: oceanographic implications, *Radiocarbon, 31*, 510-522., 1989.

Bard, E., H. Bruno, M. Arnold, L. Montaggioni, G. Cabioch, G. Faure and F. Rougerie, Deglacial sea-level record from Tahiti corals and the timing of global meltwater discharge, *Nature 382*, 241-244, 1996.

Blanke, B. and P. Delecluse, Variability of the tropical Atlantic Ocean simulated by a general circulation model with two different mixed layer physics, *J. Phys. Oceanogr., 23*, 1,363-1,388, 1993.

Bhushan, R., S. Chakraborty and S. Krishnaswami, Physical Research Laboratory (Chemistry) Radiocarbon Date List-I, *Radiocarbon, 36*, 251-256, 1994.

Bhushan, R., B.L.K. Somayajulu, S. Chakraborty, and S. Krishnaswami, Radiocarbon in the Arabian Sea water column: Temporal variations in bomb C-14 inventory since the GEOSECS and CO2 air-sea exchange rates, *J. Geophys. Res*., *105*, 14273-14282, 2000.

Broecker, W.S. and T.H. Peng, Gas exchange rates between air and sea, *Tellus, 26,* 21-35, 1974.

Broecker, W.S., S. Sutherland, W. Smethie, T.H. Peng, and G. Ostlund, Oceanic radiocarbon: Separation of the natural and bomb components, *Global Biogeochem. Cycles, 9*, 263-288, 1995.

Brown, T. A., G.W. Farwell, P.M. Grootes, F.H. Schmidt, and M. Stuiver, Intra-annual variability of the radiocarbon content of corals from the Galapagos-Islands, *Radiocarbon, 35*, 245-251, 1993.

Charles, C.D., D.E. Hunter, and R.G. Fairbanks, Interaction between the ENSO and the Asian Monsoon in a coral record of tropical climate, *Science, 277*, 925-928, 1997.

Cole, J.E., R.B. Dunbar, T.R. McClanahan, and K.A. Muthiga, Tropical Pacific forcing of decadal SST variability in the western Indian Ocean over the past two centuries, *Science, 287*, 617-619, 2000.

Druffel, E. M. and T. W. Linick, Radiocarbon in annual coral rings of Florida, *Geophys. Res. Lett., 5*, 913-916., 1978.

Druffel, E. M., Banded corals: changes in oceanic C-14 during the Little Ice-Age, *Science, 218*, 13-19, 1982.

Doney , S.C., K. Lindsay, K. Caldeira, J.-M. Campin, H. Drange, J.-C. Dutay, M. Follows, Y. Gao, A. Gnanadesikan, N. Gruber, A. Ishida, F. Joos, G. Madec, E. Maier-Reimer, J.C. Marshall, R.J. Matear, P. Monfray, A. Mouchet, R. Najjar, J.C. Orr, G.-K. Plattner, J. Sarmiento, R. Schlitzer, R. Slater, I.J. Totterdell, M.-F. Weirig, Y. Yamanaka, and A. Yool, Evaluating global ocean carbon models: The importance of realistic physics. Global Biogeochemical Cycles, 2004 (in press).

Druffel, E.M., and H.E. Suess, On the radiocarbon record in banded corals: exchange parameters and net transport of $^{14}CO_2$ between atmosphere and surface ocean, *J. Geophys. Res., 88*, 1271-1280, 1983.

Druffel, E. R. M., Decade time scale variability of ventilation in the North-Atlantic : high-Precision measurements of bomb radiocarbon in banded corals, *J. Geophys. Res., 94,* 3,271-3,285, 1989.

Druffel, E. R. M., Pulses of rapid ventilation in the North Atlantic surface ocean during the past century, *Science, 275,* 1,454-1,457, 1997.

Druffel, E. R. M., S. Griffin, T.P. Guilderson, M. Kashgarian, J. Southon, and D.P. Schrag, Changes of subtropical North Pacific radiocarbon and correlation with climate variability, *Radiocarbon, 43*, 15-25, 2001.

Duffy, P.B., and K. Caldeira, A three-dimensional model calculation of ocean uptake of bomb ^{14}C and implications for the global budget of bomb ^{14}C, *Global Biogeochem. Cycles, 9*, 373-375, 1995.

Duffy, P. B., D. E. Eliason, A.J. Bourgeois, and C.C. Covey, Simulation of bomb radiocarbon in 2 global ocean general-circulation models, *J. Geophys. Res., 100,* 22,545-22,563, 1995a.

Duffy, P.B., P. Eltgroth, A. J. Bourgeois, and K. Caldeira, Effect of improved subgrid scale transport of tracers on uptake of bomb radiocarbon in the GFDL ocean general circulation model, *Geophys. Res. Lett., 22,* 1,065-1,068, 1995b.

Duffy, P. B., K. Caldeira, J. Selvaggi, and M.I. Hoffert, Effects of subgrid-scale mixing parameterizations on simulated distributions of natural C-14, temperature, and salinity in a three-dimensional ocean general circulation model, *J. Phys. Oceanogr., 27*, 498-523, 1997.

Duffy, P.B., M. E. Wickett, and K. Caldeira, Effect of horizontal grid resolution on the near-equilibrium solution of a global ocean/sea-ice model, *J. Geophys. Res., 18,* 3075, 2002.

Dutay, J.-C., J. L. Bullister, S.C. Doney, J.C. Orr, R. Najjar, K. Caldeira, J.-M. Champin, H. Drange, M. Follows, Y. Gao, N. Gruber, M.W. Hecht, A. Ishida, F. Joos, K. Lindsay, G. Madec, E. Maier-Reimer, J.C. Marshall, R.J. Matear, P. Monfray, G.-K. Plattner, J. Sarmiento, R. Schlitzer, R. Slater, I.J. Totterdell, M.-F. Weirig, Y. Yamanaka and A. Yool, Evaluation of ocean model ventilation with CFC-11: comparison of 13 global ocean models, *Ocean Modeling, 4,* 89-120, 2002.

Dutta K., R. Bhushan R, and B.L.K. Somayajul, ΔR correction values for the northern Indian Ocean, *Radiocarbon, 43*, 483-488, 2001.

England, M. and S. Rahmstorf, Sensitivity of ventilation rates and radiocarbon uptake to subgrid-scale mixing in ocean models, *J. Phys. Oceanogr., 29*, 2,802-2,827, 1999.

Enting, I. G., T. M. Wigley and M. Heimann, Future emissions and concentrations of carbon dioxide: Key ocean/atmosphere/land analyses. Division of Atmospheric Research Technical Paper No. 31, CSIRO, Australia, pp. 120, 1994.

Fieux, M., C. Andrie, P. Dececluse, A.G. Iladhude, A. Kartavtseff, F. Mantisi, R. Molcard, and J.C. Swallow, Measurement within the Pacific and Indian Oceans throughflow region, *Deep-Sea Res.,41,* 1091-1130, 1994.

Fine, R., Direct evidence using tritium data for the throughflow from the Pacific into the Indian-Ocean, *Nature, 315*, 478-480, 1985.

Follows, M.J. and J.C. Marshall, On models of bomb ^{14}C in the North Atlantic, *J. Geophys. Res., 101*, 22,577-22,582, 1996

Gaspar, P., Y. Gregoris, and J.M. Lefevre, A simple eddy kinetic-energy model for simulations of the oceanic vertical mixing-tests at station Papa and long-term upper ocean study site, *J. Geophys. Res., 95*, 16,179-16,193, 1990.

Gargett, A. E., Vertical eddy diffusivity in the ocean interior, *J. Mar. Res., 42,* 359-393, 1984.

Gent, P. and J. McWilliams, Isopycnal mixing in ocean circulation models, *J. Phys. Oceanagr., 20,* 150-155, 1990.

Gnanadesikan, A., R.D. Slater, N. Gruber, and J.L. Sarmiento, Ocean vertical exchange and new production: a comparison between models and observations, *Deep-Sea Res. II, 49*, 363-401, 2002.

Goosse, H., E. Deleersnijder, T. Fichefet, and M.H. England, Sensitivity of a global coupled ocean-sea ice model to the parameterization of vertical mixing, *J. Geophys. Res., 104*, 13,681-13,695, 1999.

Grumet, N.S., T.P. Guilderson and R.B. Dunbar, Pre-bomb radiocarbon variability inferred from a Kenyan coral record, *Radiocarbon, 44,* 581-590, 2002a.

Grumet, N. S., T. P. Guilderson, and R.B. Dunbar, Meridional transport in the Indian Ocean traced by coral radiocarbon, *J. Mar. Res., 60*, 725–742, 200b.

Grumet N.S., N. Abram, J.W. Beck, R.B. Dunbar, M.K. Gagan, and T.P. Guilderson, Coral radiocarbon record of interannual variability in wind-induced upwelling along the coast of Sumatra, Indonesia, 2004, *J. Geophys. Res*., *109*, C05003, 2004.

Guilderson, T. P. and D. P. Schrag, Abrupt shift in subsurface temperatures in the tropical Pacific associated with changes in El Nino, *Science, 281*, 240-243, 1998.

Guilderson, T. P., D. P. Schrag, et al. Radiocarbon variability in the western equatorial Pacific inferred from a high-resolution coral record from Nauru Island, *J. Geophys. Res. 103*, 24,641-24,650, 1998.

Guilderson, T. P., K. Caldeira, and P.B. Duffy, Radiocarbon as a diagnostic tracer in ocean and carbon cycle modeling, *Global Biogeochem. Cycles, 14*, 887-902, 2000.

Hessheimer, V., M. Heimann and I. Levin, Radiocarbon evidence for a smaller oceanic carbon dioxide sink than previously believed, *Nature, 370*, 201-203, 1994.

Jain, A., H. Kheshgi, M.I. Hoffert, and D.J. Wuebbles, Distribution of radiocarbon as a test of global carbon-cycle models, *Global Biogeochem. Cycles, 9*, 153-166, 1995.

Key, R.M., Changes in the Pacific Ocean distribution of radiocarbon, 1997 U.S. WOCE Report, U.S. WOCE Implementation Rep. No. 9, U.S. WOCE Office, College Station TX,5-8, June, 1997.

Key, R.M. and P.D. Quay, U.S. WOCE Indian Ocean Survey, *Final Report for radiocarbon, Ocean Tracers Laboratory, Tech. Rep.* # 02-1. Atmospheric and Oceanic Sciences Program, Princeton Univ., Princeton, NJ, 2002.

Large, W. G., J. C. McWilliams, and S.C Doney, Oceanic vertical mixing- A review and a model with a nonlocal boundary-layer parameterization, *Revs. Geophys. 32*, 363-403, 1994.

Large, W., G. Danabasoglu, S.C Doney, and J.C. McWilliams, Sensitivity to surface forcing and boundary layer mixing in a global ocean model: Annual-mean climatology, *J. Phys. Oceanagr., 27*, 2,418-2,447, 1997.

Levitus, S., and T.P. Boyer, World Ocean Atlas 1994, Volume 4: Temperature. NOAA Atlas NESDIS 4, U.S. Department of Commerce, NOAA, NESDIS, 1994.

Maier-Reimer, E., U. Mikolajewicz, and K. Hasselmann, Mean circulation of the Hamburg LSG OGCM and its sensitivity to the thermohaline surface forcing, *J Phys. Oceanogr., 23*, 731-757, 1993.

McCulloch, M.T., A.W. Tudhope, T.M. Esat, G.E. Mortimer, J. Chappell, B. Pillans, A.R. Chivas, and A. Omura, Coral record of equatorial sea-surface temperatures during the penultimate deglaciation at Huon Peninsula, *Science 28,* 202-204, 1999.

Najjar, R. G. and J. C. Orr, Biotic-HOWTO Internal OCMIP Report. Gif-sur-Yvette, France, LSCE/CEA Saclay, 15, 1999.

Nydal, R., Radiocarbon in the ocean, *Radiocarbon, 42*, 81-98, 2000.

Orr, J. C., E. Maier-Reimer, U. Mikolajewicz, P. Monfray, J.L. Sarmiento, J.R. Toggweiler, N.K. Taylor, J. Palmer, N. Gruber, C.L. Sabine, C. Le Quere, R.M. Key, and J. Boutin, Estimates of anthropogenic carbon uptake from four three-dimensional global ocean model, *Global Biogeochem. Cycles, 15*, 43-60, 2001.

Orr, J. C., Global Ocean Storage of Anthropogenic Carbon (GOSAC), EC Environment and Climate Programme (Contract ENV4-CT97-0495) Final Report. Gif-sur-Yvette, Cedex, France, (IPSL/CNRS), 129, 2002.

Ostlund, H. G., and C. Grall. 1991. Indian Ocean radiocarbon: data from the INDIGO 1, 2, and 3 cruises. Oak Ridge National Laboratory, DOE, Oak Ridge, TN.

Sabine, C.L., R.M. Key, K.M. Johnson, F.J. Millero, A. Poisson, J.L. Sarmiento, D.W.R. Wallace and C.D. Winn, Anthropogenic CO2 inventory of the Indian Ocean, *Global Biogeochem. Cycles, 13*, 179-198, 1999.

Rayner,

Rodgers, K. B., M. A. Cane, and D.P. Schrag, Seasonal variability of sea surface $\Delta^{14}C$ in the equatorial Pacific in an ocean circulation model, *J. Geophys. Res., 102*, 18,627-18,639, 1997.

Rodgers, K. B., D. P. Schrag, M.A. Cane, and N.H. Naik, The bomb C-14 transient in the Pacific Ocean, *J. Geophys. Res., 105,* 8,489-8,512, 2000.

Schlitzer, R., Applying the adjoint method for biogeochemical modeling: export of particulate organic matter in the world ocean. In: Inverse Methods in Global Biogeochemical Cycles, pp. 107-124, 1999.

Schlitzer, R. Carbon export fluxes in the Southern Ocean: results from inverse modeling and comparison with satellite-based estimates, *Deep-Sea Res. II, 49*, 1623-1644, 2002.

Somayajulu, B., R. Bhushan, and P. Narvekar, Delta C-14, Sigma CO_2 and salinity of the western Indian Ocean deep waters: Spatial and temporal variations, *Geophys. Res. Lett.*, *26*, 2869-2872. 1999

Southon, J., M. Kashgarian, M. Fontugne, B. Metivier, and W. W. S. Yim. 2002. Marine reservoir corrections for the Indian Ocean and Southeast Asia, *Radiocarbon*, *44*, 167-180 2002)

Stuiver, M. and H.A. Polach, Discussion reporting of ^{14}C data, *Radiocarbon, 19*, 355-363, 1997.

Stuiver, M. and P. Quay, Atmospheric C-14 changes resulting from fossil-fuel CO2 release and cosmic-ray flux variability, *Earth Planet. Sci. Lett., 53*, 349-362, 1981.

Swart, P.K., G. Healy, L. Greer, M. Lutz, A. Saied, D. Anderegg, R.E. Dodge, and D. Rudnick, The use of proxy chemical records in coral skeletons to ascertain past environmental conditions in Florida Bay, *Estuaries, 22*, 384-397, 1999.

Toggweiler, J.R. and S. Trumbore, Bomb-test ^{90}Sr in Pacific and Indian Ocean surface water as recorded by banded corals, *Earth Planet. Sci. Lett.*, *74*, 306-314, 1985

Toggweiler, J. R., K. Dixon, and K. Bryan, Simulations of radiocarbon in a coarse-resolution world ocean model .2. Distributions of bomb-produced C-14, *J. Geophys. Res., 94*, 8,243-8,264, 1989.

Veronis, G., Model of world ocean circulation.1.1 Wind-driven, 2-layer, *J. Mar. Res. 31,* 228-288, 1973.

Wickett, M.E., K. Caldeira, and P. B. Duffy, Effect of horizontal grid resolution on simulations of oceanic CFC-11 uptake and direct-injection of anthropogenic CO_2, *J. Geophys. Res., 108*, 3189, 2003.

Wijffels, S., J. Sprintall, M. Fieux, and N. Bray, The JADE and WOCE I10/IR6 throughflow sections in the southeast Indian Ocean. Part 1: water mass distribution and variability, *Deep-Sea Res., 49*, 1341-1362, 2002.

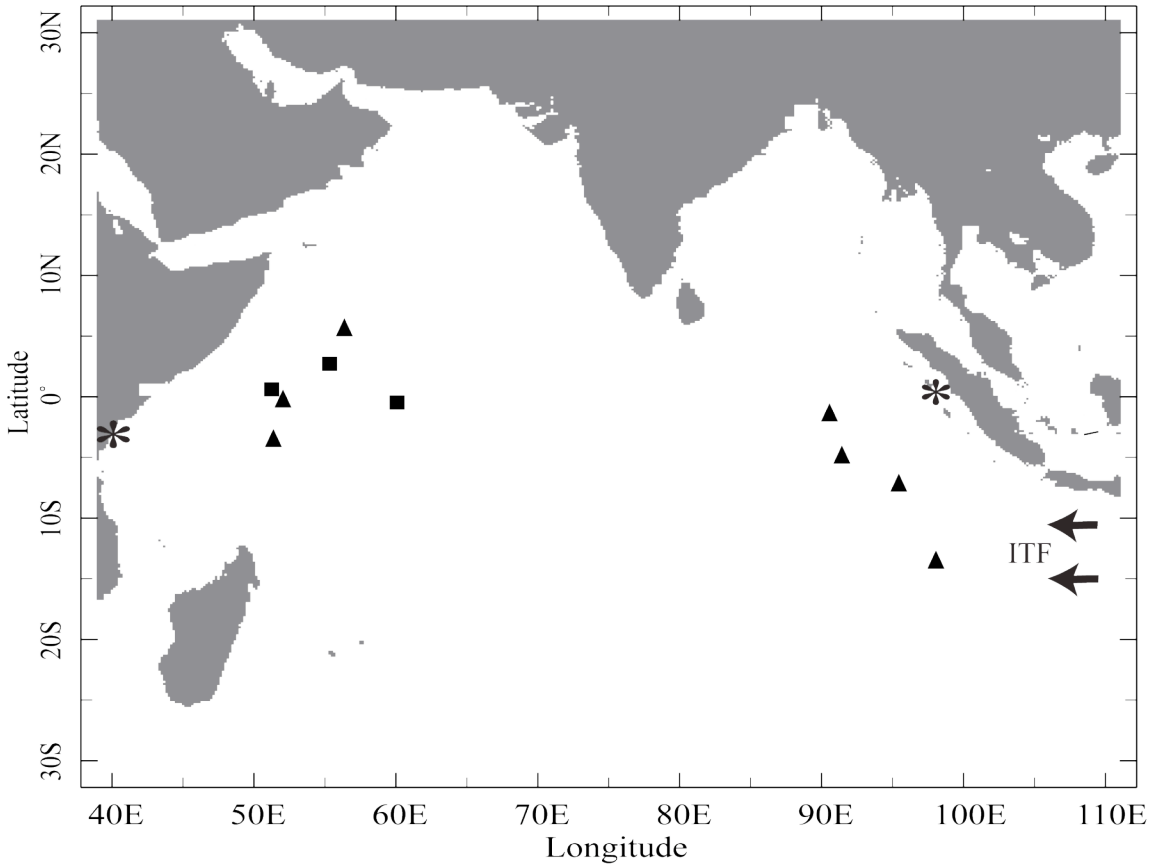
30N
20N
10N
0°
10S
20S
30S
Latitude
40E
50E
60E
70E
80E
90E
100E
110E
Longitude
ITF

Figure 1

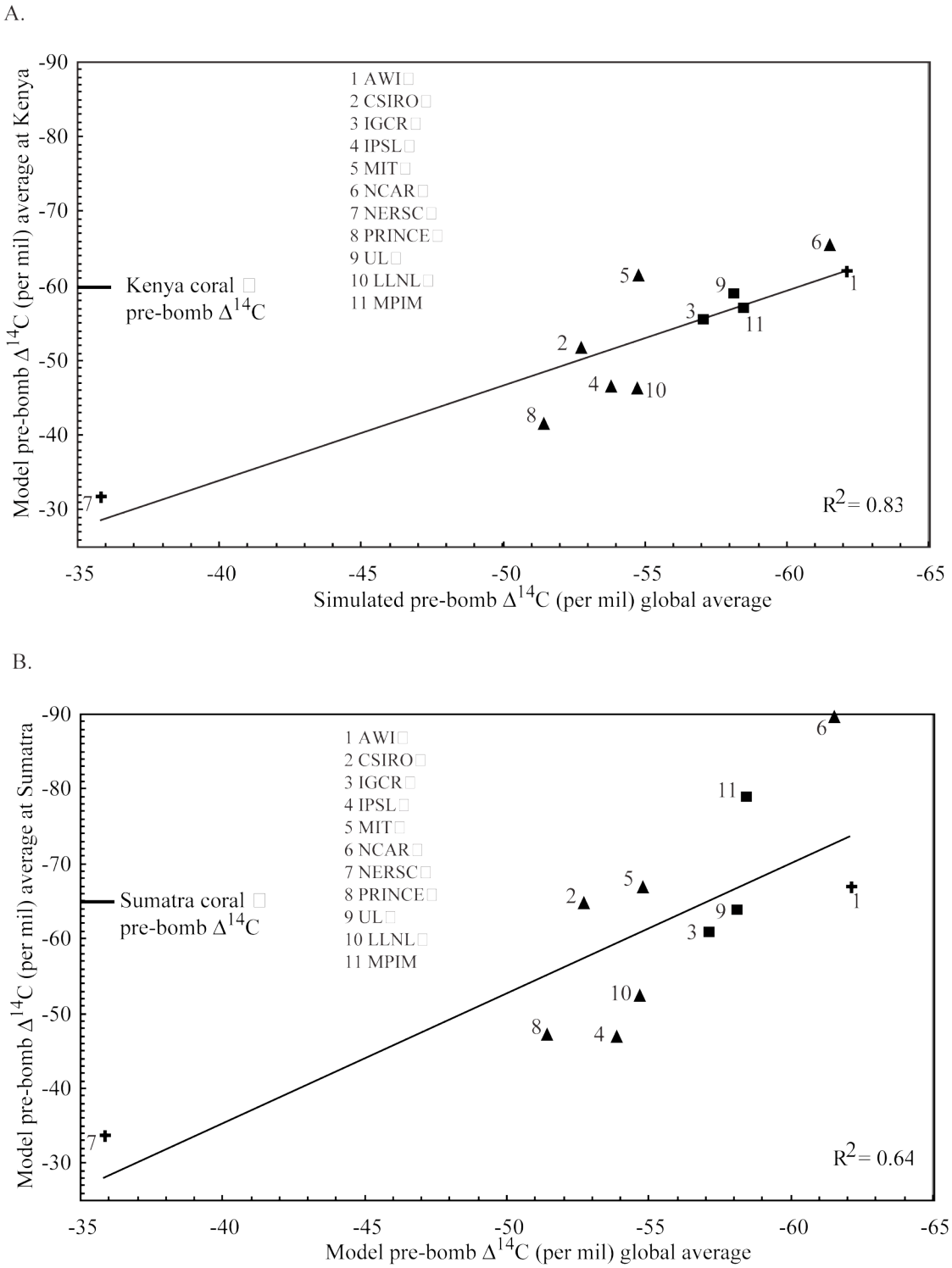
A.
Model pre-bomb Δ14C (per mil) average at Kenya
Simulated pre-bomb Δ14C (per mil) global average
Kenya coral
pre-bomb Δ14C
1 AWI
2 CSIRO
3 IGCR
4 IPSL
5 MIT
6 NCAR
7 NERSC
8 PRINCE
9 UL
10 LLNL
11 MPIM
R2= 0.83
B.
Model pre-bomb Δ14C (per mil) average at Sumatra
Model pre-bomb Δ14C (per mil) global average
Sumatra coral
pre-bomb Δ14C
R2= 0.64

Figure 2

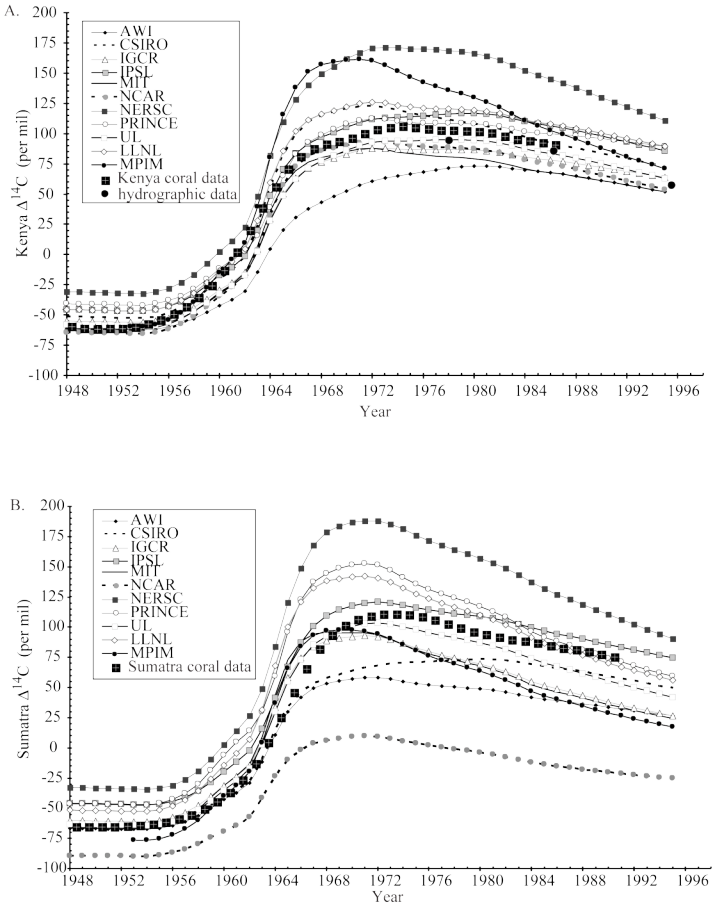
A.
AWI
CSIRO
IGCR
IPSL
MIT
NCAR
NERSC
PRINCE
UL
LLNL
MPIM
Kenya coral data
hydrographic data
Kenya Δ14C (per mil)
Year
B.
AWI
CSIRO
IGCR
IPSL
MIT
NCAR
NERSC
PRINCE
UL
LLNL
MPIM
Sumatra coral data
Sumatra Δ14C (per mil)
Year

Figure 3

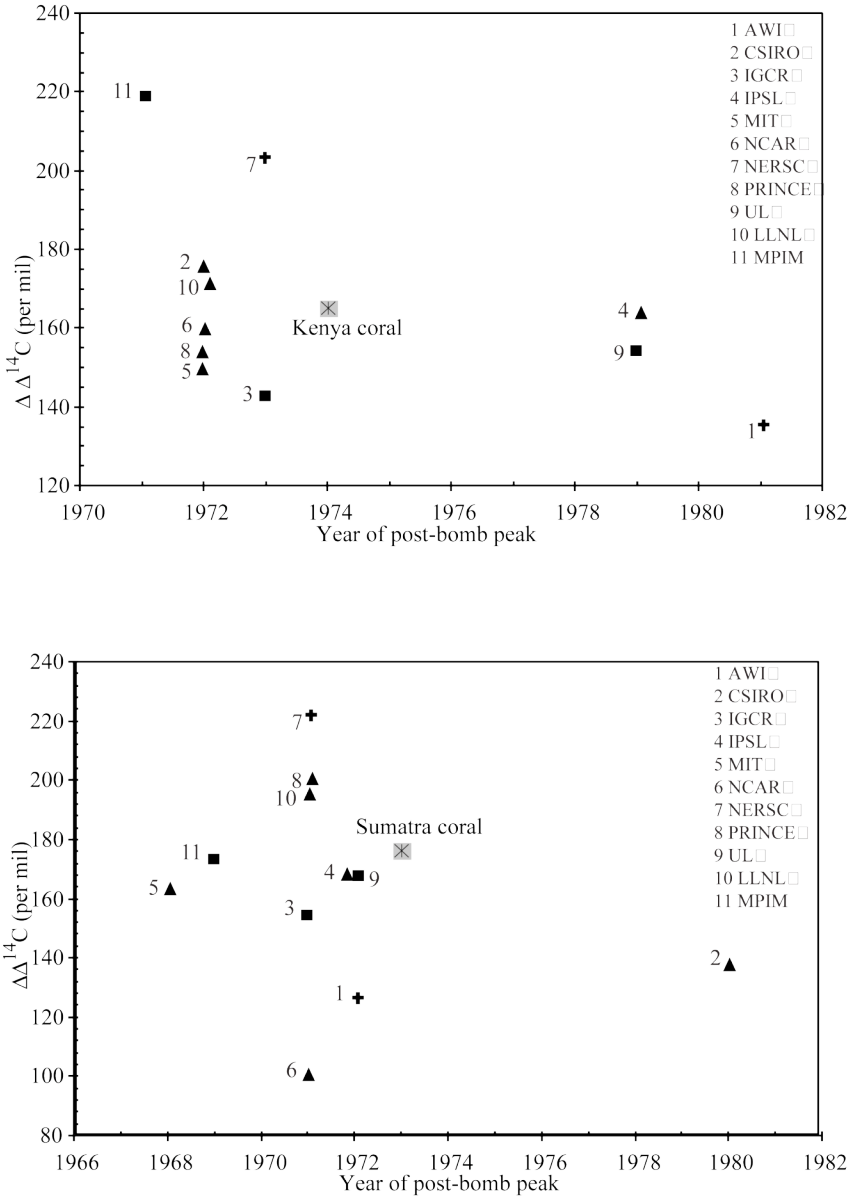
1 AWI
2 CSIRO
3 IGCR
4 IPSL
5 MIT
6 NCAR
7 NERSC
8 PRINCE
9 UL
10 LLNL
11 MPIM
Kenya coral
Sumatra coral
Δ Δ14C (per mil)
Year of post-bomb peak

Figure 4

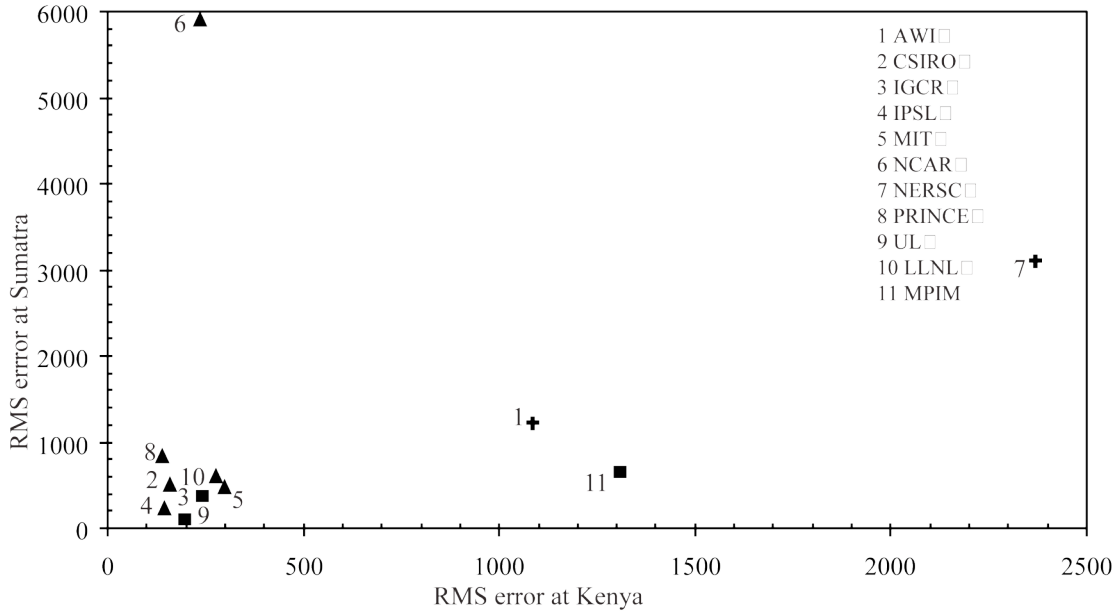

Figure 5

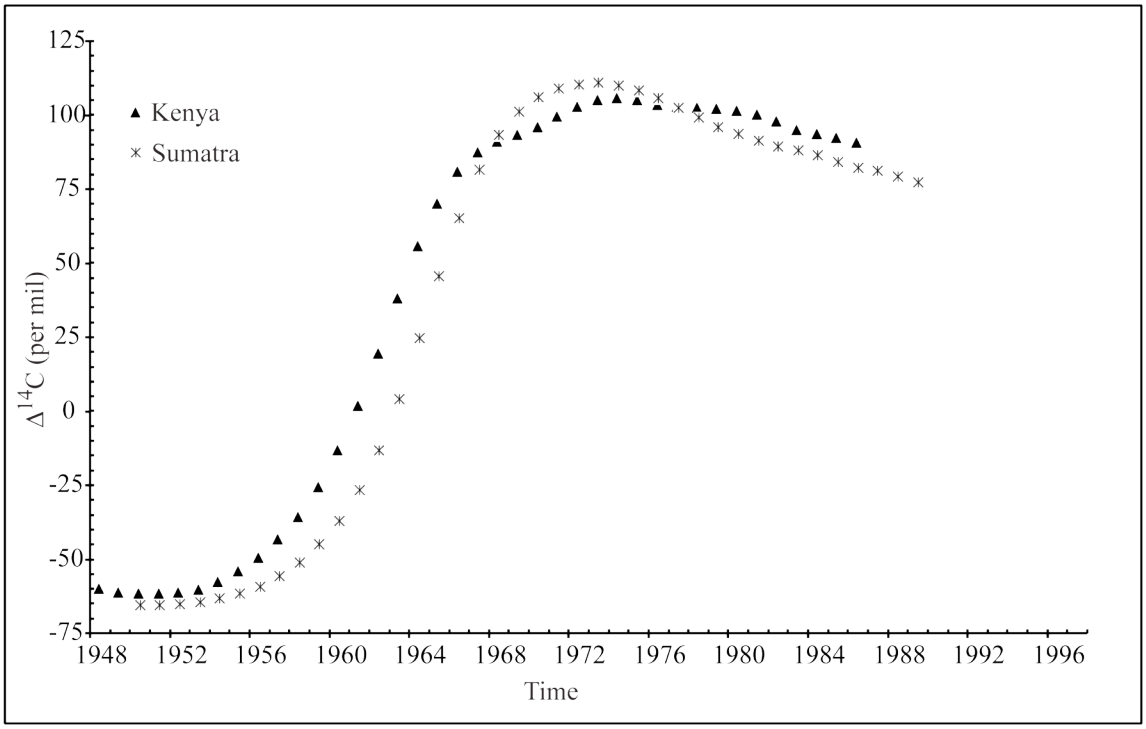

Figure 6

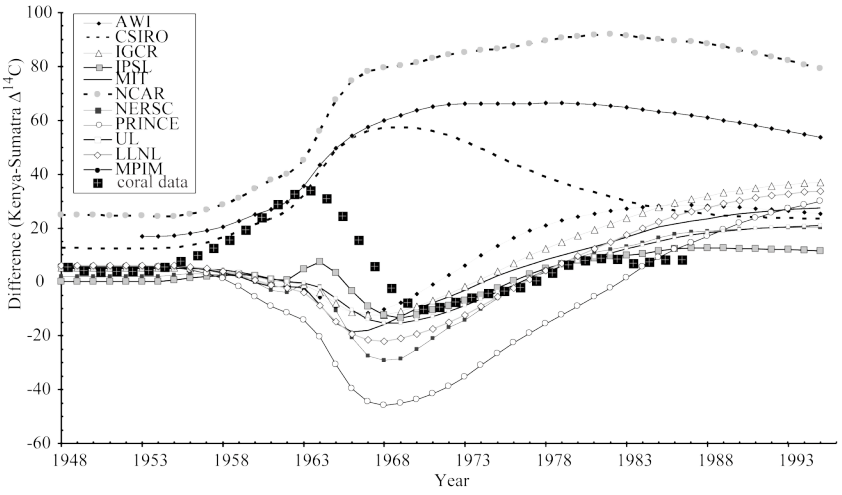

Figure 7

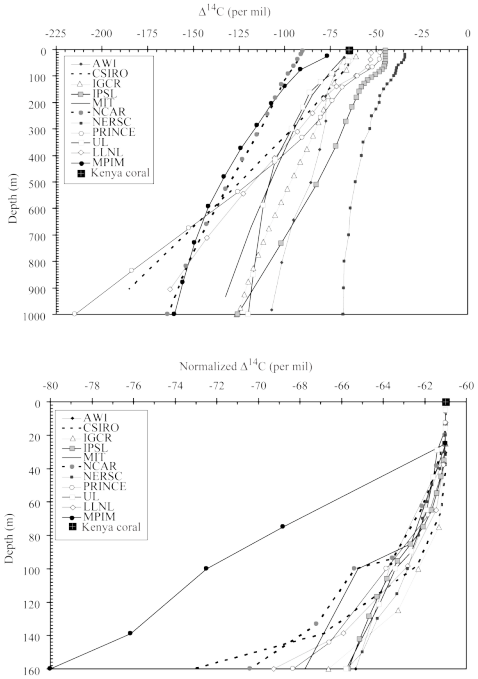

Figure 8

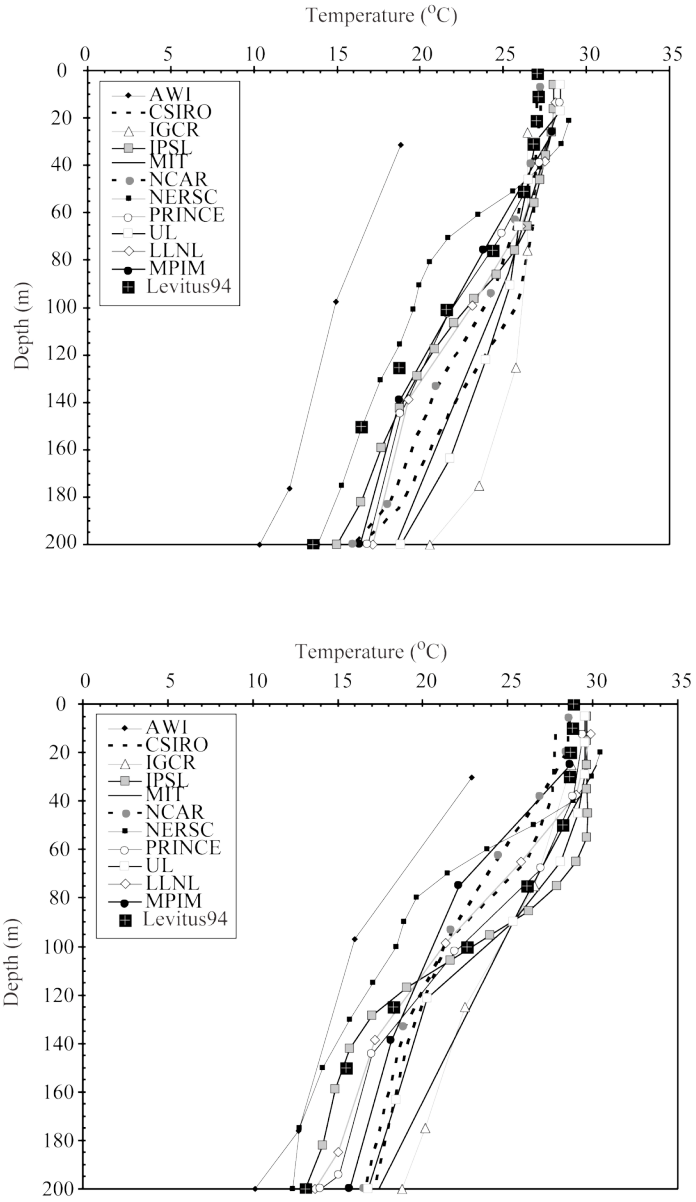
Temperature (°C)
0
5
10
15
20
25
30
35
Depth (m)
0
20
40
60
80
100
120
140
160
180
200
AWI
CSIRO
IGCR
IPSL
MIT
NCAR
NERSC
PRINCE
UL
LLNL
MPIM
Levitus94
Temperature (°C)
Depth (m)
AWI
CSIRO
IGCR
IPSL
MIT
NCAR
NERSC
PRINCE
UL
LLNL
MPIM
Levitus94

Figure 9